Mutual heavy ion dissociation in peripheral collisions at ultrarelativistic energies

I. A. Pshenichnov,[1,*] J. P. Bondorf,[2] I. N. Mishustin,[2,3] A. Ventura,[4,5,†] and S. Masetti[4]

[1]*Institute for Nuclear Research, Russian Academy of Science, RU-117312 Moscow, Russia*
[2]*Niels Bohr Institute, DK-2100 Copenhagen, Denmark*
[3]*Kurchatov Institute, Russian Research Center, RU-123182 Moscow, Russia*
[4]*Italian National Agency for New Technologies, Energy and the Environment, I-40129 Bologna, Italy*
[5]*National Institute for Nuclear Physics, Bologna Section, Italy*

We study mutual dissociation of heavy nuclei in peripheral collisions at ultrarelativistic energies. Earlier this process was proposed for beam luminosity monitoring via simultaneous registration of forward and backward neutrons in zero degree calorimeters at the Relativistic Heavy Ion Collider (RHIC) at Brookhaven National Laboratory. Electromagnetic dissociation of heavy ions is considered in the framework of the Weizsäcker-Williams method and simulated by the RELDIS code. Photoneutron cross sections measured in different experiments and calculated by the GNASH code are used as input for the calculations of dissociation cross sections. The difference in results obtained with different inputs provides a realistic estimation for the systematic uncertainty of the luminosity monitoring method. Contributions to simultaneous neutron emission due to grazing nuclear interactions is calculated within the abrasion model. A good description of the CERN SPS experimental data on Au and Pb dissociation gives confidence in the predictive power of the model for AuAu and PbPb collisions at the RHIC and the Large Hadron Collider at CERN.

I. INTRODUCTION

The study of a form of strongly interacting matter, the so-called quark-gluon plasma, is at the core of current and future experimental programs at the Relativistic Heavy Ion Collider (RHIC) at Brookhaven National Laboratory (BNL) [1] and the Large Hadron Collider (LHC) at CERN [2]. Although colliders give well-known advantages compared to the fixed target experiments, the kinematics of ultrarelativistic heavy-ion collisions at colliders creates certain complications in the beam monitoring as well as in the identification of collision events.

Due to the geometrical factor $2\pi b$, where b is the impact parameter, the number of central nuclear collisions ($b\approx 0$) is relatively very small in the whole set of the collisions with nuclear overlap, $b \lesssim R_1 + R_2$ (R_1 and R_2 are the nuclear radii). Moreover, in peripheral collisions without direct overlap of nuclear densities, $b > R_1 + R_2$, one or both nuclei may be disintegrated by the long-range electromagnetic forces. This process of electromagnetic dissociation (ED) is a well-known phenomenon [3,4]. The properties of central and peripheral collisions are very different and should be studied separately. The ED events are less violent than the collisions with the participation of strong interactions. Namely, the average particle multiplicities are essentially lower [5,6] and the main part of nucleons and mesons is produced in projectile and target fragmentation regions, very far from the midrapidity region.

Calculations show [3,5,7] that the ED cross section in collisions of heavy nuclei at the RHIC and LHC by far exceeds the dissociation cross section due to the direct nuclear

overlap. In AuAu and PbPb collisions at such energies many neutrons can be produced in the ED process [5]. Among other interesting phenomena, one may expect a complete disintegration of nuclei induced by the electromagnetic fields of collision partners [6]. This phenomenon is very well known in nuclear reactions as ''multifragmentation'' [8].

Several operational problems of heavy-ion colliders are connected with the high rate of the ED process. On the one hand, the ED process reduces the lifetime of heavy-ion beams in colliders as compared with the proton-proton accelerator mode [1,2,7]. On the other hand, the process of simultaneous neutron emission from the collision partners, where the ED process plays a dominant role, can be useful for luminosity monitoring [9–11].

The luminosity monitoring method based on mutual dissociation has several advantages [9–11]. In particular, the beam-residual-gas interaction events can be strongly suppressed in favor of the beam-beam events by the condition that a pair of neutrons should be detected in coincidence by each arm of the calorimeter. The cross section of mutual neutron emission can be calculated in the framework of conventional theoretical models designed for describing the heavy-ion disintegration in peripheral collisions. Corresponding nuclear data, especially photoneutron emission cross sections, may be used as numerical input for such calculations. Therefore, the neutron counting rates in zero degree (very forward) calorimeters may provide an accurate measure for the heavy-ion collider luminosity.

In the present paper the neutron emission in peripheral collisions of ultrarelativistic heavy ions is considered with the aim of providing the theoretical basis for the luminosity monitoring method proposed in Refs. [9–11]. The uncertainties in results originating from uncertainties in input nuclear data and in the theoretical model itself are carefully examined. A brief review of corresponding photonuclear data is given with special attention to the publications describing data evaluation and remeasurement. Model predictions for

*Email address: pshenichnov@nbi.dk
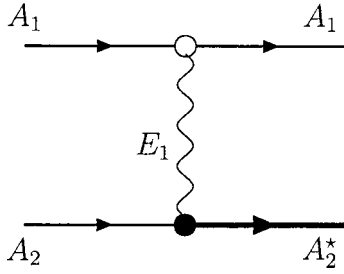†Email address: ventura@bologna.enea.it

FIG. 1. Electromagnetic excitation of one of the colliding nuclei: first order process. Open and closed circles denote elastic and inelastic vertices, respectively.

FIG. 3. Mutual electromagnetic excitation of relativistic nuclei: second order process. Open and closed circles denote elastic and inelastic vertices, respectively.

the Au and Pb fragmentation cross sections are compared with recent experimental data obtained in fixed target experiments at CERN SPS with the highest energies available thus far. This serves as an important test before extrapolating our methods to the RHIC and LHC energies.

II. EQUIVALENT PHOTON APPROACH TO SIMULTANEOUS ELECTROMAGNETIC DISSOCIATION

A. First order dissociation processes

The electromagnetic excitation of one of the collision partners A_2 followed by its dissociation is schematically shown in Fig. 1. In such a process another partner A_1 emits a photon, but remains in the ground state without any nuclear excitation. Besides this ''classical'' process, one can consider a nonclassical process where the emission of a photon is accompanied by the nuclear excitation (see Fig. 2), particularly, the giant resonance excitation. Such a lowest-order contribution to the simultaneous (mutual) excitation of the nuclei A_1 and A_2 was considered in Refs. [12,13]. Also the correction to the photon-photon luminosity function due to the inelastic photon emission was considered in Ref. [14] for $\gamma\gamma$ fusion reactions.

As shown in Refs. [12,13] (see also the discussion in Ref. [4]), the lowest-order process of simultaneous excitation of the collision partners has a small cross section. For the cases of interest, i.e., for AuAu and PbPb collisions, the cross sections for the simultaneous dipole-dipole excitation of such nuclei are 0.49 and 0.54 mb, respectively [12]. Using a rough estimation of Ref. [4], $10^{-5}A^2$ mb, one can get for the same nuclei 0.39 and 0.43 mb, respectively. From the following discussion one will see that for heavy nuclei these first order contributions (Fig. 2) are negligible compared to the second
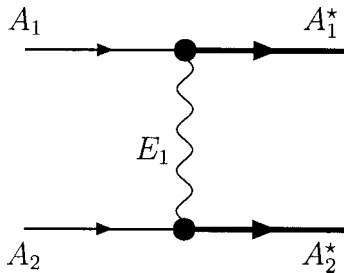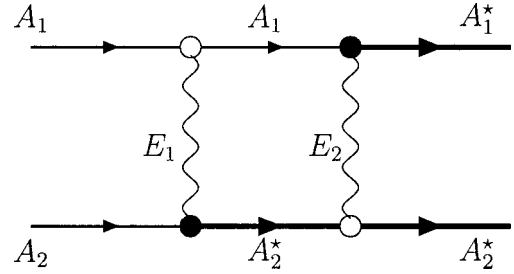
order ones (Fig. 3). The latter leading-order process with an exchange of two photons is a classically allowed mechanism. It is considered in the next section where the formalism previously used in Ref. [5] is extended to the case of mutual excitation.

B. Second order dissociation processes

Let us consider a collision of heavy ultrarelativistic nuclei at an impact parameter $b > R_1 + R_2$. The masses and charges of these nuclei are denoted as A_1, Z_1 and A_2, Z_2, respectively. Hereafter the case of equal nuclei ($A_1 = A_2 = A$, $Z_1 = Z_2 = Z$, and $R_1 = R_2 = R$) is investigated. Nevertheless, in some cases the indices are used to show explicitly which of the collision partners emits or absorbs photons.

According to the Weizsäcker-Williams method [15], the impact of the Lorentz-boosted Coulomb field of the nucleus A_1 on A_2 is treated as the absorption of an equivalent photon by the nucleus A_2 (see Fig. 1). In the rest frame of this nucleus the spectrum of virtual photons from the collision partner A_1 at impact parameter b is expressed as

$$N_{Z_1}(E_1,b) = \frac{\alpha Z_1^2}{\pi^2} \frac{\mathsf{x}^2}{\beta^2 E_1 b^2} \left(K_1^2(\mathsf{x}) + \frac{1}{\gamma^2} K_0^2(\mathsf{x}) \right). \quad (1)$$

Here α is the fine structure constant, $\mathsf{x} = E_1 b/(\gamma\beta\hbar c)$ is an argument of the modified Bessel functions of zero and first orders K_0 and K_1, $\beta = v/c$, and $\gamma = (1-\beta^2)^{-1/2}$ is the Lorentz factor of the moving charge Z_1. If the Lorentz factor of each heavy-ion beam is γ_{beam}, then $\gamma = 2\gamma_{beam}^2 - 1$ for the case of collider. Hereafter the natural units are used with $\hbar = c = 1$.

The mean number of photons absorbed by the nucleus A_2 in the collision at impact parameter b is defined by

$$m_{A_2}(b) = \int_{E_{min}}^{E_{max}} N_{Z_1}(E_1,b)\sigma_{A_2}(E_1)dE_1, \quad (2)$$

where the appropriate total photoabsorption cross section $\sigma_{A_2}(E_1)$ is used. For E_{min} one usually takes the neutron emission threshold, while the upper limit of integration is $E_{max} \approx \gamma/R$. We assume that the probability of multiphoton absorption is given by the Poisson distribution with the mean multiplicity $m_{A_2}(b)$ defined by Eq. (2).

FIG. 2. Mutual electromagnetic excitation of relativistic nuclei: first order process. Closed circle denotes inelastic vertex.

Following Refs. [5,16,17], we express the cross section for the electromagnetic dissociation of *one* of the nuclei due to the absorption of a *single* photon (Fig. 1) leading to a certain dissociation channel i as

$$\sigma_1^{ED}(i) = 2\pi \int_{b_c}^{\infty} b\,db\,P_{A_2}(b), \qquad (3)$$

where the probability of dissociation at impact parameter b is defined as

$$P_{A_2}(b) = e^{-m_{A_2}(b)} \int_{E_{min}}^{E_{max}} dE_1 N_{Z_1}(E_1,b)\sigma_{A_2}(E_1)f_{A_2}(E_1,i), \qquad (4)$$

and $f_{A_2}(E_1,i)$ is the branching ratio for the considered channel i in the absorption of a photon with energy E_1 on nucleus A_2. The choice of a critical impact parameter b_c, which separates the domains of nuclear and electromagnetic interactions, will be discussed in Sec. IV D. Let us turn now to the mutual dissociation process shown in Fig. 3. The corresponding graph may be constructed from two graphs of the single dissociation by interchanging the roles of "emitter" and "absorber" at the secondary photon exchange. Several assumptions have to be made to obtain an expression for the mutual dissociation cross section.

First, we suppose that the emitted photon with energy $E_1 \lesssim E_{max}$ does not change essentially the total energy $E_A = \gamma M_A$ of the emitting nucleus, where M_A is the nuclear mass. This can be justified by estimating the ratio

$$r = \frac{E_{max}}{E_A} \approx \frac{1}{R M_A}, \qquad (5)$$

which is close to 10^{-4} for heavy nuclei. Therefore, the kinematical conditions for the secondary photon exchange are very similar to those for the primary one, and there are no correlations between the energies of the primary and secondary photons E_1 and E_2. In other words, the primary and secondary photon exchanges may be considered as independent processes even if they take place in the same collision during a short-term overlap of the Lorentz-contracted Coulomb fields of the colliding nuclei. Second, the equivalent photon spectrum from the excited nucleus A_2^* in the notations of Fig. 3, is the same as the spectrum from the nucleus in its ground state A_2. This follows from the fact that at ultrarelativistic energies the collision time is much shorter then the characteristic deexcitation time during which a nucleus changes its initial charge via proton emission or fission.

Following these assumptions, one can express the cross section for the *mutual* dissociation of nuclei A_1 and A_2 (Fig. 3) to channels i and j, respectively, as

$$\sigma_m^{ED}(i|j) = 2\pi \int_{b_c}^{\infty} b\,db\,P_{A_1}(b)P_{A_2}(b). \qquad (6)$$

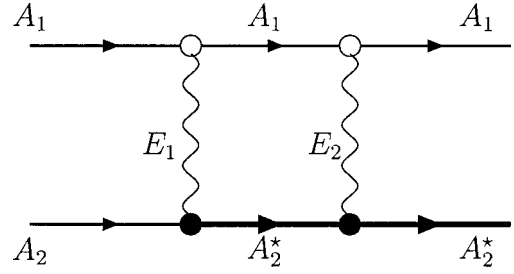Substituting Eq. (4) for each of the nuclei and changing the order of integration, one obtains

FIG. 4. Electromagnetic excitation of a single nucleus: second order process. Open and closed circles denote elastic and inelastic vertices, respectively.

$$\sigma_m^{ED}(i|j) = \int_{E_{min}}^{E_{max}} \int_{E_{min}}^{E_{max}} dE_1 dE_2 \mathcal{N}_m(E_1,E_2)$$
$$\times \sigma_{A_2}(E_1)\sigma_{A_1}(E_2)f_{A_2}(E_1,i)f_{A_1}(E_2,j), \qquad (7)$$

where the spectral function $\mathcal{N}_m(E_1,E_2)$ for mutual dissociation is introduced,

$$\mathcal{N}_m(E_1,E_2) = 2\pi \int_{b_c}^{\infty} b\,db\,e^{-2m(b)} N_{Z_1}(E_1,b)N_{Z_2}(E_2,b). \qquad (8)$$

Conditions $A_1 = A_2 = A$ and $Z_1 = Z_2 = Z$ were used in Eqs. (7) and (8), as it is usually in heavy-ion colliders, and therefore $m_{A_1}(b) = m_{A_2}(b) = m(b)$. Nevertheless, the dissociation channels i and j may be different for each of the nuclei even in such a case.

Several remarks may be made concerning Eqs. (7) and (8). Compared to another process of the second order dissociation of a single nucleus (see Fig. 4) some points of similarity may be found. Indeed, expressions given in Ref. [5] for the corresponding cross section $\sigma_2^{ED}(i)$ of the second order process are as follows:

$$\sigma_2^{ED}(i) = \int_{E_{min}}^{E_{max}} \int_{E_{min}}^{E_{max}} dE_1 dE_2 \mathcal{N}_2(E_1,E_2)\sigma_{A_2}(E_1)$$
$$\times \sigma_{A_2}(E_2)f_{A_2}(E_1,E_2,i), \qquad (9)$$

$$\mathcal{N}_2(E_1,E_2) = \pi \int_{b_c}^{\infty} b\,db\,e^{-m(b)} N_{Z_1}(E_1,b)N_{Z_1}(E_2,b). \qquad (10)$$

However, there is an important difference in the definitions of branching ratios $f_{A_2}(E_1,i)$, $f_{A_1}(E_2,j)$ compared with $f_{A_2}(E_1,E_2,i)$, since the former are for the absorption of two photons by *two different* nuclei leading to certain dissociation channels i and j, while the latter is for the absorption of two photons by a *single* nucleus leading to a channel i. Another difference is due to an additional factor of $2e^{-m(b)}$ in Eq. (7) compared with Eq. (9). It comes from the fact that Eq. (7) contains the product of the Poisson probabilities for the single photon absorption for the collision with impact parameter b,
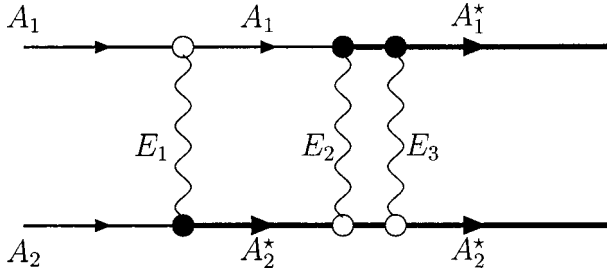
FIG. 5. Mutual electromagnetic excitation of relativistic nuclei: next-to-leading-order contribution with single and double photon exchange processes. Open and closed circles denote elastic and inelastic vertices, respectively.

$$P_{A_1}(b)P_{A_2}(b)=m^2(b)e^{-2m(b)}=2e^{-m(b)}P_A^{(2)}(b), \quad (11)$$

while $P_A^{(2)}(b)=m^2(b)e^{-m(b)}/2$ is the Poisson probability for the double photon absorption [5,16]. Results for partial cross sections of mutual dissociation will be presented and discussed in Sec. VI.

C. Next-to-leading-order processes of mutual dissociation

The second order process, which is shown in Fig. 3 and considered in Sec. II B, is the leading-order mechanism of mutual electromagnetic dissociation. This is confirmed by the calculations of the corresponding total cross sections for the leading order (LO), Fig. 3 and next-to-leading-order (NLO) processes, Figs. 5 and 6.

Following the assumption that the probability of multiphoton absorption is given by the Poisson distribution with the mean multiplicity $m_A(b)$ of Eq. (2), one has for the LO process shown in Fig. 3

$$\sigma_m^{ED}(\text{LO})=2\pi\int_{b_c}^{\infty}bdbm_A^2(b)e^{-2m_A(b)}. \quad (12)$$

Here the case of equal masses and charges of collision partners is considered, i.e., $A_1=A_2=A$ and $Z_1=Z_2=Z$.

For the NLO process with the exchange of three photons (NLO$_{12}$), Fig. 5, the total cross section is given by

$$\sigma_m^{ED}(\text{NLO}_{12})=2\pi\int_{b_c}^{\infty}bdb\frac{m_A^3(b)}{2}e^{-2m_A(b)}. \quad (13)$$
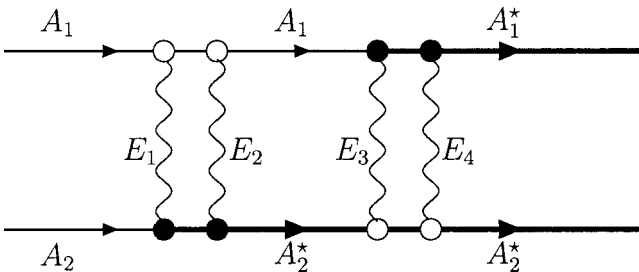

FIG. 6. Mutual electromagnetic excitation of relativistic nuclei: next-to-leading-order contribution with two double photon exchange processes. Open and closed circles denote elastic and inelastic vertices, respectively.

A complementary process (NLO$_{21}$) with the excitation of another nucleus A_2 via double photon absorption is equally possible and has the same cross section.

Another NLO process of mutual dissociation is due to exchange of four photons (NLO$_{22}$), Fig. 6, and its cross section can be written as

$$\sigma_m^{ED}(\text{NLO}_{22})=2\pi\int_{b_c}^{\infty}bdb\frac{m_A^4(b)}{4}e^{-2m_A(b)}. \quad (14)$$

Finally, one can calculate the sum of all contributions using the prescription of Ref. [11],

$$\sigma_m^{ED}(\text{tot})=2\pi\int_{b_c}^{\infty}bdb(1-e^{-m_A(b)})^2. \quad (15)$$

Since for each of the ions the probability of collision without photon exchange is equal to $e^{-m_A(b)}$, Eq. (15) is evident.

Calculations of $\sigma_m^{ED}(\text{tot})$, and $\sigma_m^{ED}(\text{LO})$, $\sigma_m^{ED}(\text{NLO})$, and cross sections for specific dissociation channels $\sigma_m^{ED}(i|j)$, with and without NLO corrections, were performed by the modified RELDIS code, which contains now a special simulation mode for the mutual electromagnetic dissociation process. Our results for the total dissociation cross sections in electromagnetic and nuclear interactions are given in Table I. These cross section values are in good agreement with results of other authors.

The total cross sections for mutual electromagnetic dissociation given in Table I are much lower than the cross sections for single dissociation. However, even the former values are found to be comparable to the total nuclear dissociation cross sections, see Table I.

As one can see, the ratios between the first and second order processes are very different for single and mutual dissociation. The first order dissociation process (with the exchange of a single photon) can be safely neglected in considering the mutual dissociation of heavy nuclei at ultrarelativistic energies.

Table I contains also the cross sections for the LO process $\sigma_m^{ED}(\text{LO})$. As one can see, the LO mechanism gives $\sim 70\%$ and $\sim 60\%$ of the $\sigma_m^{ED}(\text{tot})$ at RHIC and LHC energies, respectively. The sum of the NLO contributions to the total cross section gives additionally ~ 25–27%. Therefore, at RHIC energies, for example, the remaining contribution of $\sim 5\%$ (or ~ 0.2 b) is due to exotic triple excitations.

Finally, σ_m^{ED} and $\mathcal{N}_m$ written for the LO mutual dissociation process, Eqs. (7) and (8), can be easily generalized to the case of different NLO processes. However, the resulting expressions are lengthy and we do not give them here for brevity's sake.

III. ABRASION MODEL FOR MUTUAL DISSOCIATION IN NUCLEAR COLLISIONS

Several nucleons can be abraded from collision partners in grazing nuclear collisions. We are interested in a situation when only few nucleons are removed. This is the case when nuclear densities overlap weakly and mainly nuclear periphery is involved in the interaction.

TABLE I. Total cross sections (barn) of single and mutual dissociation calculated by the RELDIS code, abrasion model, and by other authors for AuAu and PbPb collisions at the RHIC and LHC.

	Dissociation process	First order	Second order	All contributions
	Single electromagnetic	82	1.78	83.8
65+65 A GeV AuAu at RHIC	Mutual electromagnetic		2.5	3.6
	Nuclear			7.29
	Single electromagnetic	93.2	1.86	95.1 88[a] 95[b]
100+100 A GeV AuAu at RHIC	Mutual electromagnetic	0.39×10^{-3} [c] 0.49×10^{-3} [d]	2.6	3.8 3.9[e]
	Nuclear			7.29 7.09[e]
	Single electromagnetic	212	3	215 214[a] 220[b]
2.75+2.75 A TeV PbPb at LHC	Mutual electromagnetic	0.43×10^{-3} [c] 0.54×10^{-3} [d]	3.9	6.2 7.15[e]
	Nuclear			7.88

[a]Reference [3].
[b]Reference [7].
[c]Reference [4].
[d]Reference [12].
[e]Reference [11].

The cross section for the abrasion of a nucleons from the projectile (A_1,Z_1) in a collision with the target (A_2,Z_2) may be derived from the Glauber multiple scattering theory [18],

$$\sigma^{nuc}(a)=\binom{A_1}{a}\times 2\pi\int_0^{b_c}bdb(1-P(b))^a P(b)^{A_1-a}.$$
(16)

Here $P(\vec{b})$ is calculated as the overlap of projectile $\rho_1(\vec{r})$ and target $\rho_2(\vec{r})$ densities in the collision with impact parameter b,

$$P(\vec{b})=\int d^2\vec{s}D_1(\vec{s})\exp(-A_2\sigma_{NN}D_2(\vec{s}+\vec{b})),$$
(17)

where the nuclear thickness functions,

$$D_{1,2}(\vec{s})=\int_{-\infty}^{+\infty}d\mathbf{z}\rho_{1,2}(\vec{s},\mathbf{z}),$$
(18)

are introduced. In our calculations the nuclear density functions are approximated by Fermi functions,

$$\rho_{1,2}(r)=\frac{\rho_o}{1+\exp\left(\dfrac{r-r_o A_{1,2}^{1/3}}{d}\right)},$$
(19)

where r_o is a parameter that defines the nuclear half-density radius $R_o=r_o\times A^{1/3}$, and $d=0.54$ fm is the diffuseness parameter. The choice of these and other important parameters of the model, the integration cutoff parameter b_c and the total nucleon-nucleon (NN) cross section σ_{NN}, are discussed in Sec. IV D.

The above expressions determine only the number of nucleons removed from the projectile and do not specify how many protons or neutrons were knocked out. Further assumptions are needed to determine the charge-to-mass ratio of the residual nucleus and hence the numbers of protons z and neutrons n abraded from the initial nucleus (see also the discussion in Refs. [19,20]).

In the present work we use the so-called hypergeometrical model [19,20], assuming that each removed projectile nucleon has a N_1/A_1 probability ($N_1=A_1-Z_1$) of being a neutron,

$$\sigma^{nuc}(n,z)=\frac{\binom{Z_1}{z}\binom{N_1}{n}}{\binom{A_1}{a}}\sigma^{nuc}(a). \tag{20}$$

In other words this means that there is no correlation at all between the proton and neutron distributions and the abrasion process removes protons and neutrons from the projectile nucleus in a random way.

Several physical processes that might be important in heavy-ion collisions, were neglected in this model. The excited residual nucleus created due to the abrasion process should undergo its deexcitation on the second ablation step. On this step more neutrons may be emitted via evaporation. However, as it was noticed in Ref. [19], the excitation energies obtained on the abrasion step due to removal of one or two nucleons are generally not sufficient for intensive particle evaporation. Therefore, for the cases of interest, i.e., $1n$ and $2n$ dissociation channels, the ablation step can be neglected.

The abrasion of nucleons from projectile and target proceeds via high-energy collisions between nucleons. Nucleon-antinucleon pairs may be created in such interactions and neutrons may be present in these pairs. However, as one can find in a compilation [21], even at high energies $\sim 100A$ GeV, the relative rate of such pair production is not so high, $\sim 5\%$. Because of this, we do not consider such processes in calculations of the neutron emission cross sections.

Knocked-out nucleons can also suffer a final state interaction with spectators [19]. We believe that this process is less important at high energies compared with intermediate energies of $\sim 0.1-1$ A GeV. For the latter case the escape probability is estimated to be $P_{esc}\sim 0.5-0.75$ for peripheral collisions of heavy nuclei [22]. The momenta of recoil nucleons may be comparable with the Fermi momentum of intranuclear nucleons and their angular distribution is very wide so that they can be easily captured by one of the spectators. The situation is different at high energies, where the transverse momenta of collided nucleons are typically large, of the order of 0.5 GeV, and therefore their subsequent capture is less probable. Other effects like a finite hadronization length may further reduce the secondary interaction probability. Therefore, we assume that in peripheral collisions at the RHIC and LHC the probability for each of the collided nucleons to escape the residual nuclei is close to unity, $P_{esc}\sim 1$.

As we will show in Sec. V, the above-mentioned simplifications do not lead to noticeable disagreements with experimental data when the removal of one, two, or three nucleons is considered. It means that either the above-mentioned physical effects are negligible, or they compensate for each other in peripheral nuclear collisions with the removal of only a few nucleons. However, the predictions of the present model for more central collisions with the removal of many nucleons should be taken with care.

This simple abrasion model can be easily extended to the case of mutual dissociation. The cross section for the removal of n_1 neutrons and z_1 protons from the projectile (N_1,Z_1) *simultaneously* with the removal of n_2 neutrons and z_2 protons from the target (N_2,Z_2), $(N_2=A_2-Z_2)$ may be written as

$$\sigma_m^{nuc}(n_1,z_1|n_2,z_2)=\frac{\binom{Z_1}{z_1}\binom{N_1}{n_1}}{\binom{A_1}{a}}\times\sigma^{nuc}(a)\times\frac{\binom{Z_2}{z_2}\binom{N_2}{n_2}}{\binom{A_2}{a}}. \tag{21}$$

Since the number of nucleon-nucleon collisions in such a process is assumed to be equal to a, the condition $z_1+n_1=a=z_2+n_2$ holds.

Using this condition for the process of mutual dissociation with given numbers of neutrons n_1 and n_2 removed from the projectile and target nuclei, respectively, one has finally

$$\sigma_m^{nuc}(n_1|n_2)=\sum_{z_1}\sigma^{nuc}(n_1,z_1)\frac{\binom{Z_2}{n_1+z_1-n_2}\binom{N_2}{n_2}}{\binom{Z_2+N_2}{z_1+n_1}}. \tag{22}$$

Here the cross section for the single abrasion process $\sigma^{nuc}(n_1,z_1)$, given by Eqs. (16) and (20), was used.

IV. INPUT DATA FOR HEAVY-ION DISSOCIATION CALCULATIONS

As shown in Sec. II, the photonuclear cross sections are used as input data in calculations of the electromagnetic dissociation cross sections. This is verified by the coherent nature of the photon emission by the collision partner as a whole. Since these photons represent the Lorentz-boosted Coulomb fields of original nuclei, their virtuality is very small, $Q^2 \lesssim 1/R^2$, i.e., these photons are almost real. Therefore, one can use the photonuclear reaction data obtained in experiments with real monoenergetic photons and apply theoretical models describing such photonuclear reactions.

The accuracy of the mutual dissociation cross section calculation depends heavily on the quality of the data and parameters used as input. As we found, for example, the mutual dissociation cross section is more sensitive to the proper choice of the critical impact parameter b_c and to the input photonuclear cross sections than the single dissociation cross section. The input data and model parameters are discussed in detail in the following sections.
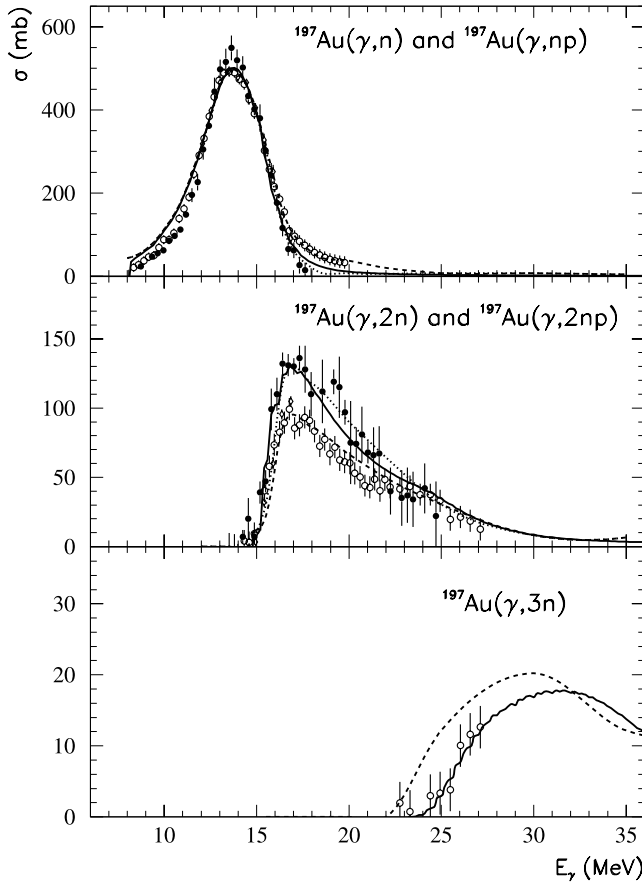
FIG. 7. Photoneutron cross sections for gold. Open and closed circles are, respectively, Saclay (Ref. [23]) and Livermore (Ref. [26]) data rescaled according to Ref. [31]. GNASH code results are presented by solid line. RELDIS results are given by dashed and dotted lines for variants with and without inclusion of the direct $1n$ emission, respectively.
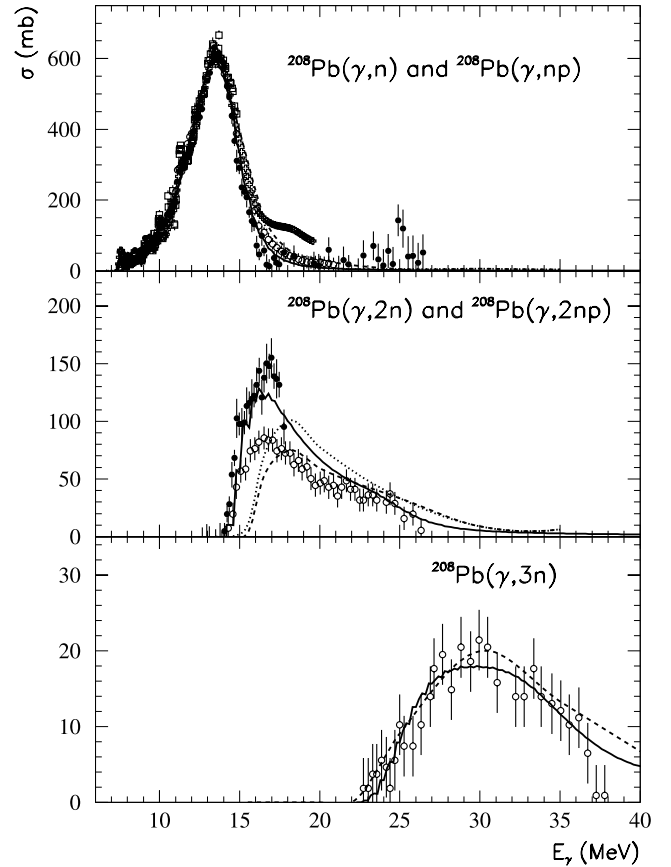

FIG. 8. Photoneutron cross sections for lead. Open and closed circles are, respectively, Saclay (Ref. [23]) and Livermore (Ref. [26]) data rescaled according to Ref. [31]. Crosses, Saratov data [32]; squares, Moscow evaluated data (Ref. [33]). Other notations are the same as in Fig. 7.

A. Photoneutron cross sections measured in experiments with real photons

Over the years, the photoneutron cross sections for different nuclei have been measured with monoenergetic photons at Saclay [23–25] and Livermore [26]. Data on different cross sections obtained in these and other laboratories were collected in compilations of Refs. [27,28].

Concerning the nuclei of interest, ^{197}Au and ^{208}Pb, the detailed data were obtained mainly for (γ,n) and $(\gamma,2n)$ reactions, while less detailed data exist for $(\gamma,3n)$ and $(\gamma,4n)$ reactions, see Refs. [23,26]. The measurements were performed in the photon energy region $6 \leq E_\gamma \leq 35$ MeV, where the excitation of giant resonances plays a dominant role, see Figs. 7 and 8. At such energies, the emission of charged particles $(p,d,^3\mathrm{He},^4\mathrm{He})$ is suppressed by a high Coulomb barrier of heavy nuclei. Therefore, the sum of partial cross sections for all neutron multiplicities $\sigma(\gamma,n) + \sigma(\gamma,2n) + \sigma(\gamma,3n) + \sigma(\gamma,4n)$ nearly coincides with the total photoabsorption cross section. Each of the inclusive cross sections $\sigma(\gamma,in)$ for the emission of i neutrons includes a small contribution from the channels with charged particles $(\gamma,in\,p)$, $(\gamma,in\,2p)$, $\ldots$. At the same time chan-

nels such as (γ,p), $(\gamma,2p)$ were neglected altogether. According to Ref. [24], this leads to a small systematic error $\sim 3-5\,\%$ in the total photoabsorption cross section measured at low energies via the neutron detection.

Above the giant resonance region, at $35 \leq E_\gamma \leq 140$ MeV, the quasideuteron mechanism of photon absorption dominates. Only average characteristics of photon absorption by ^{208}Pb were measured in Saclay [24,25] in this energy region. Neutron yields $\Sigma_{i \geq 1} i\sigma(\gamma,in)$ and the cross sections for emission of at least j neutrons $\Sigma_{i \geq j}\sigma(\gamma,in)$ were obtained in addition to the mean value and the width of the neutron multiplicity distribution.

To the best of our knowledge there are no direct measurements of neutron emission cross sections and multiplicities at $E_\gamma > 30$ MeV in photoabsorption on ^{197}Au. The only attempt to deduce the average photoneutron multiplicities from the experimentally obtained average excitation energies has been made at $160 \leq E_\gamma \leq 250$ MeV in a model-dependent way [29].

For the (γ,n) channel the overall agreement between Livermore and Saclay data is good. Some inconsistency exists only in the giant resonance peak height ($\sim 3\%$ for ^{197}Au and $\sim 20\%$ for ^{208}Pb) and on the right side of the peak, where

(γ,n) and $(\gamma,2n)$ processes compete with each other, see Figs. 7 and 8. Large discrepancies are present in $(\gamma,2n)$ cross sections measured in different experiments, both in shape and normalization, up to $\sim 50\%$ for the ^{208}Pb target.

Several attempts at data evaluation and remeasurements have been made to reduce these discrepancies. Based on the observation that the total photoneutron yields $\sigma(\gamma,n) + 2\sigma(\gamma,2n) + 3\sigma(\gamma,3n)$ obtained in Livermore and Saclay experiments agree well, an explanation for the discrepancy was put forward in Ref. [30]. It was attributed to the different neutron multiplicity sorting procedures adopted in different laboratories. As was concluded in Ref. [30], the neutron multiplicity sorting procedure adopted at Saclay was not correct since some of the $(\gamma,2n)$ events were interpreted as pairs of (γ,n) events.

In 1987 new measurements were made in Livermore [31], where it was found that the previously reported Livermore [26] and Saclay [23] results have to be rescaled. As was recommended in Ref. [31], the Saclay data of Ref. [23] for both ^{197}Au and ^{208}Pb nuclei have to be used with the correction factor of 0.93. We follow this prescription in using photonuclear cross section data in our RELDIS code. However, such a correction is not widely accepted and the authors of Refs. [7,10,11] use uncorrected Saclay data.

Some new $(\gamma,2n)$ cross section data were obtained in Ref. [31] for ^{197}Au and ^{208}Pb. For the ^{197}Au nucleus, $(\gamma,2n)$ data are nearly the same as the Saclay $(\gamma,2n)$ data of Ref. [31] and the conclusion of Ref. [30] concerning the neutron multiplicity sorting procedure seems to be unconfirmed. Unfortunately, the recent data of Ref. [31] are available only up to a few MeV above the $(\gamma,2n)$ threshold and the findings of Ref. [30] cannot be completely ruled out.

One of the most recent measurements of the (γ,n) cross section for photoabsorption on ^{208}Pb was performed in Russia at Saratov University [32]. A fine structure of the low-energy wing of the giant dipole resonance (GDR) has been investigated in detail. The photoneutron cross sections were obtained from the photoneutron yield curves by means of the statistical regularization method.

An evaluation of the (γ,n) cross section for ^{208}Pb has been made at Moscow State University [33] by applying a statistical reduction method. Because of systematic uncertainties in calibration and normalization, the general characteristics of the measured (γ,n) cross section (the energy integrated cross sections, weighted-mean values) are different in different measurements [23,24,26]. In the reduction method of Ref. [33] the renormalization corrections were introduced for both the energy and the cross section scales in order to obtain the best agreement between the general characteristics of the (γ,n) cross section measured in different experiments.

The data obtained in Refs. [32,33] for the (γ,n) reaction on the ^{208}Pb target are also plotted in Fig. 8. Good agreement with rescaled Saclay data of Ref. [23] is found up to the $(\gamma,2n)$ threshold. Unfortunately, the $(\gamma,2n)$ reaction was beyond the scope of investigations in Refs. [32,33].

It is evident from our consideration that the calculations of electromagnetic dissociation of ultrarelativistic ^{197}Au and ^{208}Pb nuclei cannot be based exclusively on the photo-neutron cross sections measured in experiments with real photons. Additional information on photoneutron cross sections for the whole energy domain of equivalent photons $(E_{min} \leqslant E_\gamma \leqslant E_{max})$ can be obtained by using theoretical models of photoabsorption. This is particularly indispensable for dissociation channels with an emission of many neutrons $(\geqslant 3)$ and charged particles $p,d,t,\alpha, \dots$.

B. Evaluation of photoneutron cross sections using the GNASH code

One of the two photonuclear reaction models used in the present work is the GNASH code [34]. It is very precise in describing low-energy neutron emission data [35], however, it can be used only up to the pion production threshold at $E_\gamma \leqslant 140$ MeV. Within this model the photoabsorption process is modeled through the excitation of the giant dipole resonance (GDR) at lower energies and the quasideuteron (QD) mechanism at higher energies.

The photoabsorption cross section in the whole energy range from the threshold for neutron emission up to 140 MeV is thus written in the form [35]

$$\sigma_A(E_\gamma) = \sigma_{GDR}(E_\gamma) + \sigma_{QD}(E_\gamma), \tag{23}$$

where σ_{GDR} is given by a Lorentzian curve with parameters taken from GDR systematics [28] and corrected according to Ref. [31]. The latter term σ_{QD} is related by a Levinger-type model to the experimental deuteron photodisintegration cross section σ_d [36],

$$\sigma_{QD}(E_\gamma) = L \frac{NZ}{A} \sigma_d(E_\gamma) F(E_\gamma), \tag{24}$$

where N, Z, and A are, respectively, the neutron, proton, and mass number of the corresponding nucleus. The Levinger parameter L is equal to 6.5, and $F(E_\gamma)$ is a Pauli-blocking factor, which reduces the free deuteron cross section $\sigma_d(E_\gamma)$ by taking into account the Pauli blocking of the excited neutron and proton in the nuclear medium. In Ref. [36], F was derived in the form of a multidimensional integral, approximated in the energy range 20–140 MeV by a polynomial expression,

$$F(E_\gamma) = 8.3714 \times 10^{-2} - 9.8343 \times 10^{-3} E_\gamma + 4.1222$$
$$\times 10^{-4} E_\gamma^2 - 3.4762 \times 10^{-6} E_\gamma^3 + 9.3537 \times 10^{-9} E_\gamma^4, \tag{25}$$

and by an exponential one outside the considered energy range,

$$F(E_\gamma) = \begin{cases} \exp(-73.3/E_\gamma), & E_\gamma < 20 \text{ MeV}, \\ \exp(-24.2/E_\gamma), & E_\gamma > 140 \text{ MeV}. \end{cases}$$

Thus, $F(E_\gamma)$ tends to zero if E_γ goes to zero, and to unity if E_γ goes to infinity and is continuous with Eq. (25) at 20 and 140 MeV [35].

Finally, the experimental deuteron photodisintegration cross section is given by a simple parametrization,

$$\sigma_d(E_\gamma) = 61.2(E_\gamma - 2.224)^{3/2}/E_\gamma^3, \qquad (26)$$

where E_γ is expressed in MeV, as in the previous formulas, and σ_d in mb.

Due to the correlation between intranuclear nucleons in the absorption on a quasideuteron pair, the initial particle-hole configuration is assumed to be $2p1h$ rather than $2p2h$, see Ref. [35]. In the GNASH code the initial interaction characterized by the total cross section of Eqs. (23)–(25) is followed by the preequilibrium emission of fast nucleons described by the exciton model [34,35]. Finally, when the nuclear system comes to equilibrium, sequential evaporation of particles is considered within the Hauser-Feshbach formalism [35].

GNASH code results for (γ,n), $(\gamma,2n)$, and $(\gamma,3n)$ cross sections are shown in Figs. 7 and 8 for ^{197}Au and ^{208}Pb nuclei, respectively. Calculations describe (γ,n) and $(\gamma,3n)$ data very well. Taking into account existing disagreements between the results of different measurements of $(\gamma,2n)$ cross sections, one can conclude that the GNASH results fall in between the Saclay [23] and Livermore data [26] for ^{208}Pb and very close to Livermore data for ^{197}Au, which seems to be satisfactory for both cases. Therefore, one can use in Eq. (7) the photonuclear cross sections $\sigma_A(E_\gamma)$ and branching ratios $f(E_\gamma,i)$ calculated by the GNASH code to estimate the mutual electromagnetic dissociation cross section $\sigma_m^{ED}(i|j)$. The influence of a constraint $E_\gamma < E_{max} = 140$ MeV will be discussed in Sec. VI.

C. Neutron emission simulated by cascade and evaporation codes

Branching ratios for neutron emission in photonuclear reactions $f(E_\gamma,i)$ can be calculated by means of the extended cascade-evaporation-fission-multifragmentation model of photonuclear reactions [37] in the whole range of equivalent photon energies. Some details of the calculation method as well as numerous comparisons with experimental data used for the model verification were given in Refs. [5,6,37]. Here we describe only the general calculation scheme along with the modifications and advancements made in the model since the time when the works [5,6,37] were published.

In the RELDIS model the values of the total photoabsorption cross section to be used in Eq. (7) are taken from corresponding approximations of experimental data. In the GDR region the Lorentz curve fits were used for this purpose with parameters from Ref. [27] corrected according to the prescription of Ref. [31], as described in Sec. IV A. Above the GDR region, where the quasideuteron absorption comes into play, the total cross section is taken from the quasideuteron model of Ref. [24],

$$\sigma_{QD}(E_\gamma) = k\frac{NZ}{A}\sigma_d^{exch}(E_\gamma). \qquad (27)$$

Here σ_d^{exch} is the meson exchange part of the cross section for the deuteron photodisintegration $\gamma d \to np$, and k is an empirical constant [24].

Above the pion production threshold, at $E_\gamma \gtrsim 140$ MeV, a universal behavior $\sigma_A(E_\gamma) \propto A$ is observed (see Ref. [38] for the latest experimental data). This means that the total photoabsorption cross section per bound nucleon $\sigma_A(E_\gamma)/A$ has almost the same energy dependence for light, medium-weight, and heavy nuclei C, Al, Cu, Sn, and Pb, at least up to $E_\gamma \sim 3$ GeV. Therefore, having the data for one nucleus, one can calculate the cross section for other nuclei. However, in this energy region the universal curve $\sigma_A(E_\gamma)/A$ is very different from the values extrapolated from the cross sections on free nucleons $(Z\sigma_{\gamma p} + N\sigma_{\gamma n})/A$, which are deduced from proton and deuteron data [38]. At $E_\gamma > 3$ GeV the universal behavior breaks down, and the ratio $\sigma_A(E_\gamma)/A$ for lead is 20–25 % lower than for carbon [39,40] due to the nuclear shadowing effect. In order to approximate the total photonuclear cross sections at $E_\gamma > 3$ GeV we used recent results obtained within the framework of the Glauber-Gribov scattering theory and the generalized vector dominance model [39,40]. Such calculations describe well the general trend of experimental data obtained for high-energy photon absorption, although the data have very large uncertainties at $E_\gamma > 10$ GeV.

By comparing Table II of Ref. [5] and Table I of the present paper one can find minor differences in the total ED cross sections due to using different parametrizations of $\sigma_A(E_\gamma)/A$ at $E_\gamma > 3$ GeV. Compared with the total ED cross sections, the single or double neutron emission cross sections are even less affected by the choice of the parametrization.

The RELDIS code performs the Monte Carlo simulation of the mutual dissociation process according to the following steps. First, a pair of the energies E_1 and E_2 of the photons exchanged between the colliding nuclei is selected according to the spectral function $\mathcal{N}_m(E_1,E_2)$. Second, the photoabsorption process is generated in both nuclei leading to the formation of excited residual nuclei. Third, the deexcitation of both of the thermalized residual nuclei is simulated according to the statistical evaporation-fission-multifragmentation model [8].

The evaporation of neutrons from an excited residual compoundlike nucleus is the main process responsible for the (γ,n), $(\gamma,2n)$, $(\gamma,3n)$ channels of photoabsorption. The quality of the description of such channels is very important for precise calculations of neutron emission in the mutual dissociation process. In the present paper the standard Weisskopf evaporation scheme is used [8] with several modifications taking into account the microscopic effects of nuclear structure in the nuclear mass and level density formulas. Such effects reveal themselves in the noticeable difference, up to $\sim 10-15$ MeV for heavy closed-shell nuclei, between the values of the nuclear mass measured in experiments and those predicted by the macroscopic liquid-drop model.

Moreover, this difference in mass, the so-called shell correction, and the level density parameter are strongly correlated. For closed-shell nuclei the actual values of the level density parameter are essentially lower than the average values expressed as $A/8 - A/10$ MeV^{-1}, and these values depend noticeably on the excitation energy. Proper accounting for these effects, as well as pairing effects, is important at

TABLE II. Cross sections (barn) for ^{197}Au dissociation induced by 158A GeV Pb beams. Theoretical results are obtained by the RELDIS code and abrasion model. Experimental data are taken from Ref. [54]. RELDIS results without direct 1n emission are given in parentheses.

Dissociation channel	$\sigma_1^{ED}(i) + \sigma_2^{ED}(i)$		$\sigma^{nuc}(i)$		All contributions	
	Experiment	RELDIS code	Experiment	Abrasion model	Experiment	Theory
$i = 1n$ ^{197}Au$\rightarrow$^{196}Au$+n$	26.4$\pm$4.0	26.96 (25.09)	0.3$\pm$0.1	0.43	26.7$\pm$4.0	27.39 (25.52)
$i = 2n$ ^{197}Au$\rightarrow$^{195}Au$+2n$	4.6$\pm$0.7	4.57 (6.39)	0.13$\pm$0.04	0.13	4.7$\pm$0.7	4.70 (6.52)

low excitations $E^* \sim 10$ MeV, i.e. in the region where 1n and 2n photoemission processes occur.

The above-mentioned shell effects are most pronounced at low excitation energies, but almost disappear at $E^* > 50$ MeV, see Ref. [20] for details. Several phenomenological systematics of the level density parameter were proposed to account for such behavior, see Refs. [41–43]. Our calculations are based on results of Ref. [43] where all existing data on the level densities, decay widths, and lifetimes of excited nuclei have been analyzed in the framework of the statistical model.

However, the creation and subsequent decay of an excited compound nucleus formed after the photoabsorption in the GDR region is not the only process responsible for the neutron emission. Indeed, a giant resonance is a coherent superposition of (one-particle–one-hole) $1p1h$ excitations. A particle or a hole can interact with another nucleon and create a $2p2h$ state. Further spreading to $3p3h$ states etc. finally leads to a statistically equilibrated system, the compound nucleus. Instead of such evolution to equilibrium, a collective $1p1h$ state can decay directly by the emission of one nucleon leading to a low-lying hole state in the residual nucleus, see, for instance, Ref. [44]. After such direct 1n emission, the emission of a second neutron is generally impossible, even though the initial photon energy exceeds the 2n emission threshold. In such a way the (γ,2n) channel is suppressed in comparison with the pure statistical decay.

Although the GDR state in the ^{208}Pb nucleus decays mainly statistically, the existence of direct neutron emission has been clearly demonstrated in Ref. [45]. The process whereby a fast nucleon is emitted and the final state of the ^{207}Pb nucleus is left with low excitation energy $\leqslant 3$ MeV was identified in this experiment [45]. Evidence of direct neutron emission in photoabsorption on Au and Pb nuclei was given in Ref. [23] based on the analysis of competition between 1n and 2n emission channels. This was an independent confirmation of the findings of earlier works [46,47]

devoted to the measurements of the neutron spectra in photoabsorption on the same nuclei. An excess of fast neutrons (kinetic energy $\geqslant 4$ MeV) with respect to the predictions of the statistical evaporation model has been demonstrated and attributed to the direct emission.

In Ref. [44] a nonstatistical contribution in an excited ^{208}Pb nucleus with $10 < E^* < 30$ MeV was successfully extracted. Out of this region the nonstatistical contribution was found to be negligible. In our calculations we used the total fractions of the nonstatistical neutron emission from Au and Pb nuclei as $P_n^{dir} = 0.31$ and 0.26, respectively, evaluated from experimental data in Ref. [23]. Such values are in line with modern theoretical expectations [48] that the ratio of intensities of the direct and statistical neutron emission from photoexcited GDR in the ^{208}Pb nucleus is about ~ 0.1. In the RELDIS code the emission angles Θ of nonstatistical fast photoneutrons are generated according to the approximation $W(\Theta) = A + B\sin^2\Theta$, which is found in Ref. [47]. We assumed that the direct 1n emission takes place at $7 \leqslant E^* \leqslant 22$ MeV.

Since the adopted P_n^{dir} values have some uncertainties, we have investigated the sensitivity of results to these values. A part of the calculations was made with $P_n^{dir} = 0$, i.e. without accounting for direct emission, see Figs. 7 and 8 and Table II. As shown in Fig. 7, the (γ,2n) cross sections on gold calculated by the RELDIS code with $P_n^{dir} = 0.31$ are very close to Saclay measurements [23], while Livermore results [26] are better described with $P_n^{dir} = 0$. Therefore the difference in calculation results obtained with $P_n^{dir} = 0$ and $P_n^{dir} = 0.31$ reflects the level of experimental uncertainties.

D. Choice of cutoff parameter and nuclear density distributions

Since the nucleon-nucleon interaction has an isovector component, the interference of nuclear and electromagnetic amplitudes cannot be excluded. Such interference terms were considered in Ref. [22] and found to be small. Even for the

[197]Au nucleus colliding with heavy targets the interference correction to the single neutron removal cross section was found to be less than 0.5–0.6 % of the corresponding nuclear or electromagnetic contributions. Following this result, nuclear and electromagnetic parts of the dissociation cross section may be safely treated separately. In other words, one can add probabilities instead of coherent summation of amplitudes.

Let us consider how the probabilities of the nuclear and electromagnetic contributions should be added to obtain the total dissociation probability. At grazing impact parameters relativistic nuclei are partly transparent to each other. Hard NN collisions may be absent altogether in the case of a peripheral event with a weak overlap of diffuse nuclear surfaces, while the electromagnetic interaction may take place in this event leading to the electromagnetic dissociation. Generally, at a grazing collision either the nuclear or electromagnetic interaction, or even both of them, may occur. As an example of the latter case, a single neutron-neutron collision in the participant zone may lead to the neutron removal, while a photon may be emitted and absorbed by charged spectators in the same event.

Therefore, in a detailed theoretical model a smooth transition from purely nuclear collisions at $b \ll R_1 + R_2$ to electromagnetic collisions at $b \gg R_1 + R_2$ should take place. Such a kind of transition was considered in a "soft-sphere" model of Ref. [49]. A similar approach was adopted in Ref. [11], where the cross section for at least one type of dissociation, either nuclear, electromagnetic, or both, was written as

$$\sigma = 2\pi \int_0^\infty b\,db (\mathcal{P}^{nuc}(b) + \mathcal{P}^{ED}(b) - \mathcal{P}^{nuc}(b)\mathcal{P}^{ED}(b)), \tag{28}$$

where $\mathcal{P}^{nuc}(b)$ and $\mathcal{P}^{ED}(b)$ are, respectively, the probabilities of the nuclear and electromagnetic dissociations at a given impact parameter b. Putting explicitly the integration limits for each term, one obtains

$$\sigma = 2\pi \int_0^{b_c^{nuc}} b\,db\,\mathcal{P}^{nuc}(b) + 2\pi \int_{b_c^{ED}}^\infty b\,db\,\mathcal{P}^{ED}(b)$$
$$- 2\pi \int_{b_c^{ED}}^{b_c^{nuc}} b\,db\,\mathcal{P}^{nuc}(b)\mathcal{P}^{ED}(b). \tag{29}$$

Here the impact parameter cutoff values b_c^{nuc} and b_c^{ED} were used for the nuclear and electromagnetic interactions, respectively. However, due to several reasons a more simple expression is widely used [3,4],

$$\sigma = \sigma^{ED} + \sigma^{nuc} = 2\pi \int_0^{b_c} b\,db\,\mathcal{P}^{nuc}(b) + 2\pi \int_{b_c}^\infty b\,db\,\mathcal{P}^{ED}(b), \tag{30}$$

where a single cutoff parameter b_c was chosen as $b_c^{ED} < b_c < b_c^{nuc}$. The first reason is that with the latter condition one can effectively reduce the first and second terms of Eq. (29) without subtracting the third nuclear-plus-electromagnetic term. Numerical results based on Eqs. (29) and (30) become

similar as it was found for "sharp-cutoff" and "soft-sphere" models of Ref. [49]. Second, for heavy nuclei the difference between reasonable values of b_c^{ED}, b_c^{nuc}, and b_c turns out to be less than 1 fm. As a result, the last nuclear-plus-electromagnetic term of Eq. (29) turns out to be small. Third, with Eq. (30) one can study the nuclear and electromagnetic contributions separately. Therefore, independent parametrizations may be found in experiments for the nuclear and electromagnetic parts σ^{nuc} and σ^{ED}. This is useful for studying nuclear and electromagnetic dissociation at ultrarelativistic colliders, where the products of nuclear and electromagnetic interactions populate very different rapidity regions, namely the central rapidity region and close to the beam rapidity, respectively.

In the present paper the traditional form given by Eq. (30) is adopted with a common impact parameter cutoff b_c for nuclear and electromagnetic contributions. At relativistic energies, according to the widely used Benesh-Cook-Vary (BCV) parametrization of Ref. [22], b_c is estimated as

$$b_c = R_{BCV}[A_1^{1/3} + A_2^{1/3} - X_{BCV}(A_1^{-1/3} + A_2^{-1/3})]. \tag{31}$$

The values $R_{BCV} = 1.34$ fm and $X_{BCV} = 0.75$ were found from a fit to Glauber-type calculations of the total nuclear reaction cross sections [22].

The evidence in favor of the b_c choice according to the BCV parametrization was given in Refs. [50,51], which we mention among others. As argued in Ref. [51], using the BCV parametrization one can perfectly describe experimental data on fragment angular distributions which are very sensitive to b_c.

For calculations within the abrasion model we used the following values for the total nucleon-nucleon cross section given in Ref. [52]: $\sigma_{NN} = 40$, 50, and 90 mb at SPS, RHIC, and LHC energies, respectively. Some problems are connected with the choice of the nuclear density parameters $R_o = r_o \times A^{1/3}$ and $d = 0.54$ fm, see Sec. III. Only the nuclear charge distributions are measured in electron scattering experiments, while the neutron densities are available only from calculations. We used $r_o = 1.14$ fm as an average value between the proton and neutron distributions similar to one used in Ref. [11]. The total nuclear reaction cross sections calculated with these r_o and d values within the abrasion model are in good agreement with the approximation of experimental data found in Ref. [22]. Numerical results showing the sensitivity of the nuclear and mutual electromagnetic dissociation cross sections to the variations of the above-discussed parameters are given in Sec. VI.

V. COMPARISON WITH CERN SPS DATA

The calculated charge changing cross sections of the *single* dissociation of 158A GeV [208]Pb ions are given in Fig. 9. The LO mechanism with a single photon exchange, Fig. 1, and the NLO mechanism with a double photon exchange, Fig. 4, were taken into account.

Each proton removal process can be accompanied by neutron loss as well. The calculated cross sections given for $Z = 82$ correspond to the interaction where only neutrons are
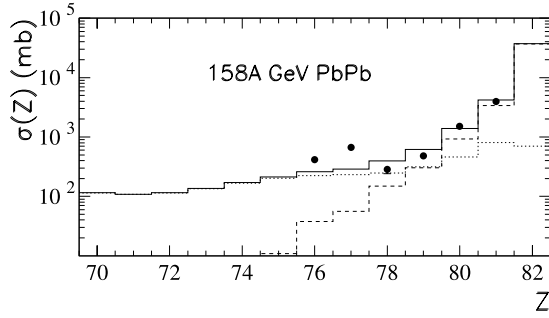
FIG. 9. Charge changing cross sections of 158 A GeV ^{208}Pb ions on the Pb target. The dashed- and dotted-line histograms are the RELDIS and abrasion model results for electromagnetic and nuclear contributions, respectively. The solid-line histogram presents the sum of both contributions. Points are experimental data from Ref. [53].

emitted. However, experimental data are absent for this channel. As one can see, the electromagnetic contribution dominates for the processes with removal of one, two, and three protons where good agreement with the experimental data of Ref. [53] is found.

Another important check of the model becomes possible with recent experimental data for Au fragmentation by ultrarelativistic Pb ions [54]. In this case the neutron emission is investigated directly. The experimental exclusive cross sections for emission of one or two neutrons are compared with theory in Table II. Also in this case the contributions from the LO and NLO processes, Figs. 1 and 4, were taken into account.

The calculations were made with and without accounting for the direct neutron emission process, i.e. with $P_n^{dir} = 0.31$ and $P_n^{dir} = 0$, respectively. The results with $P_n^{dir} = 0.31$ are in better agreement with experiment and this is especially true for the $2n$ emission channel. Therefore, we use this value in further calculations.

The predictions of the abrasion model are also in good agreement with data [54]. Therefore, our choice of the critical impact parameter b_c is justified by such a comparison. As was stressed in Sec. III, the interaction of knocked-out nucleons with spectators and the spectator deexcitation process themselves were neglected in this version of the abrasion model aimed at considering only a few nucleon removal processes. Such good agreement indicates that a simple abrasion model proposed for describing the data at ~1–10 A GeV can be used successfully at much higher energies as well.

VI. MUTUAL DISSOCIATION OF ^{197}Au AND ^{208}Pb IONS AT THE RHIC AND LHC

On the basis of the successful verifications at lower energies described in Sec. V, the model can now be extrapolated to RHIC and LHC energies. In a collider, the mutual heavy-ion dissociation process takes place at the crossing point of two beams. Downstream from this point the dissociation products can be separated by the magnetic field according to their Z/A ratio. Protons and nuclear fragments move close to the beam trajectories, while free neutrons leave the beam pipe after a dipole magnet.

TABLE III. Mutual electromagnetic dissociation cross sections for AuAu collisions at the RHIC. X and Y denote any particle, except neutrons. $\mathcal{D}$ means any dissociation channel. Calculation results are given (a) for the leading-order contribution only and (b) for the sum of leading-order and next-to-leading-order contributions.

	Cross section (mb)	(a) LO	(b) LO+NLO
	$\sigma_m^{ED}(1nX\vert 1nY)$	612	659
65+65 A GeV	$\sigma_m^{ED}(1nX\vert \mathcal{D})$	1244	1502
AuAu at RHIC	$\sigma_m^{ED}(2nX\vert \mathcal{D})$	330	446
	$\sigma_m^{ED}(3nX\vert \mathcal{D})$	148	274
	$\sigma_m^{ED}(1nX\vert 1nY)$	607	652
100+100 A GeV	$\sigma_m^{ED}(1nX\vert \mathcal{D})$	1257	1518
AuAu at RHIC	$\sigma_m^{ED}(2nX\vert \mathcal{D})$	341	461
	$\sigma_m^{ED}(3nX\vert \mathcal{D})$	155	284

At the RHIC, zero degree (very forward) calorimeters (ZDC) for each beam are located after the magnets and they are well designed for the neutron registration [9–11]. Therefore, in the following we consider mainly semi-inclusive mutual neutron emission cross sections $\sigma_m(i\vert j)$, where i and j denote corresponding channels $1nX$, $2nX$, $3nX$, ... Besides the emission of a given number of neutrons, such dissociation channels contain any number of other particles denoted as X or Y. Protons can be found most often amongst the particles emitted along with neutrons. The proton emission rates predicted by the RELDIS code were found to be in agreement with the data on Pb dissociation [53], see Sec. V. Therefore we believe that our model is accurate in estimating $\sigma_m(1nX\vert 1nY)$, $\sigma_m(1nX\vert 2nY)$, and $\sigma_m(2nX\vert 2nY)$ cross sections.

If the dissociation channel of one of the collision partners in mutual dissociation is not exactly known, one can define inclusive mutual dissociation cross sections $\sigma_m(1nX\vert \mathcal{D})$, $\sigma_m(2nX\vert \mathcal{D})$, and $\sigma_m(3nX\vert \mathcal{D})$, etc. In such notations $\mathcal{D}$ denotes an arbitrary dissociation mode of one of the nuclei.

The cross sections for some specific channels of mutual dissociation at RHIC energies are given in Table III. Compared to the total cross sections, the relative contributions of NLO processes are very different for the cross sections of $1n$, $2n$, and $3n$ emissions. As one can note, $\sigma_m^{ED}(1nX\vert 1nY)$ has a small NLO correction, ~7%, while $\sigma_m^{ED}(3nX\vert D)$ be-

TABLE IV. Sensitivity of the partial mutual electromagnetic dissociation cross sections to the variation of probability of the direct neutron emission in the $1n$ channel P_n^{dir} to the input photonuclear cross sections and to the corrections for next-to-leading-order processes. Results obtained with GNASH and RELDIS codes are given for $100+100\ A$ GeV AuAu collisions. Recommended values are presented in boldface. The prediction of Ref. [11] for $\sigma_m^{ED}(1n|1n)$ is given for comparison.

Cross section (mb)	$E_\gamma \lesssim 24$ MeV LO	$E_\gamma \lesssim 140$ MeV LO		Full range of E_γ LO+NLO	
	RELDIS $P_n^{dir}=0$	GNASH	RELDIS $P_n^{dir}=0$	RELDIS $P_n^{dir}=0$	RELDIS $P_n^{dir}=0.31$
$\sigma_m^{ED}(1nX|1nY)$	437 445[a]	430	467	549	**652**
$\sigma_m^{ED}(1nX|2nY)$ $+\sigma_m^{ED}(2nX|1nY)$	205	221	262	439	**388**
$\sigma_m^{ED}(2nX|2nY)$	21	28	38	87	**60**
$\sigma_m^{ED}(LMN)$	663	679	767	1075	**1100**

[a]Reference [11].

comes almost twice as large as its LO value if the NLO correction is included. This is due to the fact that the NLO processes shown in Figs. 5 and 6 include nuclear excitation due to double photon absorption and, particularly, the double GDR excitation process. Since the average GDR energy for Au and Pb nuclei is about 13–14 MeV, the double GDR excitation introduces, on average, 26–28 MeV excitation, which is above the $3n$ emission threshold.

Therefore, as a rule, $1n$ and $2n$ emission cross sections are less affected by including NLO corrections rather than $3n$ cross sections. The double GDR excitation process is a well-known phenomenon studied in low- and intermediate-energy heavy-ion collisions, see, for example, Ref. [55]. However, nothing is known about the multiple photon excitations of heavy ions at ultrarelativistic energies, where the key question is to what extent the distribution of probabilities for multiple excitations follows the Poisson distribution (the harmonic picture of excitations).

In order to estimate the rates of multiple excitations, including those well above the giant resonance region, the ratios $\sigma_m^{ED}(2nX|D)/\sigma_m^{ED}(1nX|1nY)$ and $\sigma_m^{ED}(3nX|D)/\sigma_m^{ED}(1nX|1nY)$ should be measured at the RHIC. Such measurements do not require a preliminary determination of the collider luminosity. As it follows from Table III, the above-mentioned ratios are remarkably reduced if the multiple excitations, and hence the NLO processes, are suppressed in mutual electromagnetic dissociation at the RHIC.

There remains still some freedom in choosing several parameters of our model. To check the sensitivity of our predictions to their variations we performed the calculations for a reasonable span of input parameters.

Table IV demonstrates the sensitivity of the mutual electromagnetic dissociation cross sections to the photonuclear cross sections used as the input. In order to demonstrate such sensitivity we used two different models to calculate such cross sections, namely, the GNASH code [34] and the photonuclear reaction model implemented in the RELDIS code

[5,37] itself. Additionally, in the latter model we used two different values for the probability of the direct neutron emission in the $1n$ channel, P_n^{dir}.

Besides the variations of the cross sections for emission of one or two neutrons, the variations of a cumulative value, the low multiplicity neutron (LMN) emission cross section defined as

$$\sigma_m(LMN) = \sigma_m(1nX|1nY) + \sigma_m(1nX|2nY)$$
$$+ \sigma_m(2nX|1nY) + \sigma_m(2nX|2nY)$$

was evaluated for several subregions of equivalent photon energies $E_\gamma < 24$ MeV, $E_\gamma < 140$ MeV, and for the full range. In the latter case the NLO processes were taken into account along with the LO mutual dissociation process. Therefore, the importance of NLO corrections can be also estimated from Table IV.

By examining Table IV, one can draw several conclusions. First, the semi-inclusive cross section $\sigma_m^{ED}(1nX|1nY) = 437$ mb calculated for the photoabsorption in the giant resonance region is very close to the exclusive value $\sigma_m^{ED}(1n|1n) = 445$ mb obtained in Ref. [11] with the same condition, $E_\gamma < 24$ MeV. Second, the calculations based on the photonuclear cross sections predicted by the GNASH code are very close to the RELDIS results for the photon energy region $E_\gamma < 140$ MeV. The difference between the RELDIS results for $E_\gamma < 24$ MeV and $E_\gamma < 140$ MeV is explained by the contribution of the quasideuteron photoabsorption mechanism to the $1n$ and $2n$ emissions. Third, the calculations that take into account the quasideuteron photoabsorption and photoreactions above the pion production threshold give about 25% enhancement in $\sigma_m^{ED}(1nX|1nY)$ if the whole energy region of equivalent photons is considered and the NLO corrections are properly taken into account. At the same time, the cross sections $\sigma_m^{ED}(1nX|2nY)$

TABLE V. Sensitivity of the mutual dissociation cross section in nuclear interactions to the variation of the r_o parameter of the nuclear density distribution. Results of the abrasion model are given for $100+100$ A GeV AuAu collisions. Recommended values are given in boldface.

Cross section (mb)	Abrasion model			
	$r_o=1.09$ $R_o=6.34$ fm	$r_o=1.12$ $R_o=6.52$ fm	$r_o=1.14$ $R_o=6.63$ fm	$r_o=1.16$ $R_o=6.75$ fm
$\sigma_m^{nuc}(1nX|1nY)$	361	364	**371**	382
$\sigma_m^{nuc}(1nX|2nY)$ $+\sigma_m^{nuc}(2nX|1nY)$	241	232	**224**	226
$\sigma_m^{nuc}(2nX|2nY)$	148	147	**142**	139
$\sigma_m^{nuc}(LMN)$	750	743	**737**	747

and $\sigma_m^{ED}(2nX|2nY)$ increase up to two and four times, respectively, compared with the values calculated at the GDR region.

The cross sections for these dissociation channels are large and such channels can be easily measured in experiments. Although the LO process of photoabsorption in the GDR region gives an important contribution, the whole range of the equivalent photon energies should be considered. Also the contributions from the NLO processes should be taken into account to obtain the realistic values of the dissociation cross sections.

One more conclusion follows from the results presented in Table IV. Calculations with $P_n^{dir}=0$ and $P_n^{dir}=0.31$ give a 10–40 % difference in specific dissociation cross sections, but the values of the LMN cross section $\sigma_m^{ED}(LMN)$ practically coincide. This cross section is very high, $\sigma_m^{ED}(LMN)$ $\sim$ 1100 mb, and thus can be used for luminosity monitoring. As was shown above in Sec. IV A, an inevitable systematic error of $\sim$ 5% should be assigned to this value due to uncertainties in the photoneutron cross sections measured in experiments.

Table V shows the sensitivity of the mutual dissociation cross section in grazing nuclear collisions to the variations of

the r_o parameter in the nuclear density distribution, Eq. (19). The parameters of neutron density distributions are not well determined and this table demonstrates possible ambiguities in nuclear dissociation cross sections caused by this fact. The cross section variations are smaller in Table V compared to Table IV, about 3–8 %. A small decrease in the r_o parameter leads to a decrease in correlated $1n$-$1n$ emission, but, on the contrary, it leads to an increase in $1n$-$2n$ and $2n$-$2n$ emission. However, the LNM cross section $\sigma_m^{nuc}(LMN)$ turns out to be more stable, within a $\sim$ 2% variation, compared to the cross sections for specific channels.

The sensitivity of the dissociation cross section in grazing nuclear collisions to the variations of the total nucleon-nucleon cross section is investigated in Table VI. The variations of the σ_{NN} in the range of 40–60 mb have only a small effect, within 4%, on the cross sections of the specific neutron emission channels. Since such variations have different signs, the influence on the cumulative value $\sigma_m^{nuc}(LMN)$ is less noticeable, below 2%.

The cross sections given in Tables V and VI for grazing nuclear collisions were found to be lower compared with the electromagnetic dissociation cross sections of Table IV. Moreover, it should be stressed that only a part of the neu-

TABLE VI. Sensitivity of the mutual dissociation cross section in nuclear interactions to the variation of the total nucleon-nucleon cross section σ_{NN}. The results of the abrasion model are given for $100+100$ A GeV AuAu collisions. Recommended values are given in boldface.

Cross section (mb)	Abrasion model		
	$\sigma_{NN}=40$ mb	$\sigma_{NN}=50$ mb	$\sigma_{NN}=60$ mb
$\sigma_m^{nuc}(1nX|1nY)$	370	**371**	374
$\sigma_m^{nuc}(1nX|2nY)$ $+\sigma_m^{nuc}(2nX|1nY)$	233	**224**	222
$\sigma_m^{nuc}(2nX|2nY)$	148	**142**	138
$\sigma_m^{nuc}(LMN)$	751	**737**	734

TABLE VII. Sensitivity of the mutual dissociation cross section in electromagnetic and nuclear interactions to the critical impact parameter b_c. The results of the RELDIS code and abrasion model are given for $100+100$ A GeV AuAu collisions. Recommended values are given in boldface.

Cross section (mb)	$R_{BCV}=1.27$ $b_c=14.45$ fm	$R_{BCV}=1.34$ $b_c=15.25$ fm	$R_{BCV}=1.41$ $b_c=16.05$ fm
$\sigma_m^{ED}(1nX\vert 1nY)$	677	**652**	629
$\sigma_m^{ED}(1nX\vert 2nY)$ $+\sigma_m^{ED}(2nX\vert 1nY)$	417	**388**	374
$\sigma_m^{ED}(2nX\vert 2nY)$	62	**60**	57
$\sigma_m^{ED}(LMN)$	1156	**1100**	1060
$\sigma_m^{nuc}(1nX\vert 1nY)$	379	**371**	390
$\sigma_m^{nuc}(1nX\vert 2nY)$ $+\sigma_m^{nuc}(2nX\vert 1nY)$	240	**224**	259
$\sigma_m^{nuc}(2nX\vert 2nY)$	141	**142**	151
$\sigma_m^{nuc}(LMN)$	760	**737**	800
$\sigma_m^{ED}(LMN)$ $+\sigma_m^{nuc}(LMN)$	1916	**1837**	1860

trons in grazing nuclear collisions is emitted at the forward or backward angles covered by the ZDC's. Therefore, an exact relation between nuclear and electromagnetic dissociation channels in each heavy-ion experiment should be only obtained by taking into account detection acceptances and trigger conditions of the corresponding experimental setup.

Table VII demonstrates the sensitivity of the mutual dissociation cross section in electromagnetic and nuclear interactions to the impact parameter cutoff b_c. This is an important input parameter, which has a noticeable influence on the final result. By changing this parameter by 5%, within the range of 14.5–16 fm, one obtains the variations of the electromagnetic dissociation cross sections within 3–8 %. Such variations of b_c shift the point, which delimits the regions of nuclear and electromagnetic interactions, below or above the domain where the overlap of diffuse nuclear boundaries takes place. In other words, assuming first $b_c\approx b_c^{ED}$ and then $b_c\approx b_c^{nuc}$ and considering the difference in final results, one can prove the possibility to use Eq. (30) instead of Eq. (29).

For example, if the cutoff value b_c becomes higher, all the ED cross sections $1n$-$1n$, $1n$-$2n$, $2n$-$2n$, and $\sigma_m^{ED}(LMN)$ become lower. The variations of the nuclear cross sections are more noticeable and have the opposite trend: such cross sections become higher by 5–15 %. Finally, as one can see in Table VII, $\sigma_m(LMN)$ variations for both types of interactions are weaker than the variations of the corresponding individual cross sections, within 3–8 %, while the sum $\sigma_m^{ED}(LMN)+\sigma_m^{nuc}(LMN)$ is altered by 1–4 % only.

Concluding the investigation of the sensitivity of the final results to the model parameters, one can note that for AuAu collisions at the RHIC $\sigma_m^{ED}(LMN)=1100$ mb and especially $\sigma_m^{nuc}(LMN)=737$ mb are more stable with respect to such variations in comparison with the individual cross sections $\sigma_m(1nX\vert 1nY)$, $\sigma_m(1nX\vert 2nY)$, and others. The same tendency was found for PbPb collisions at LHC energies

where such cross sections were found to be $\sigma_m^{ED}(LMN)=1378$ mb and $\sigma_m^{nuc}(LMN)=755$ mb. For both RHIC and LHC cases the overall uncertainty of the $\sigma_m(LMN)$ calculation method may be estimated to be at the level of 5–7 %.

The condition for heavy-ion dissociation to be mutual leads to some specific features for nuclear and electromagnetic interactions. The former interaction causes mainly symmetric or quasisymmetric dissociation. The latter makes very probable asymmetric dissociation like $(1nX\vert 5nY)$ or even $(1nX\vert 10nY)$. This feature is shown in Figs. 10 and 11 where the cross sections with one, two, or three neutrons in one arm of the ZDC setup are presented. As one can see, $(1nX\vert 10nY)$ dissociation is almost absent in nuclear collisions. This is not true for electromagnetic dissociation where the number of $(1nX\vert 10nY)$ events is approximately 1–5 % of the main dissociation channel $(1nX\vert 1nY)$.

In the RELDIS model nuclei undergo dissociation independently of each other in the electromagnetic fields. Therefore there is no correlation between the numbers of neutrons, n_1 and n_2 emitted by each of the nuclei, and asymmetric dissociations are possible along with symmetric ones. The extreme case of asymmetric dissociation is, of course, the single dissociation process. The nuclear dissociation considered in the framework of the abrasion model has different characteristic features. Namely, the numbers of emitted neutrons and protons are correlated due to the condition $z_1+n_1=z_2+n_2$, see Sec. III, and nuclear dissociation is always mutual. The latter condition was also adopted in Ref. [11].

The main results of our study are presented in Figs. 12 and 13. They show the electromagnetic and nuclear dissociation cross sections. Since $1n$ and $2n$ emissions in electromagnetic collisions are enhanced due to the GDR and QD absorption mechanisms, the corresponding strips are promi-
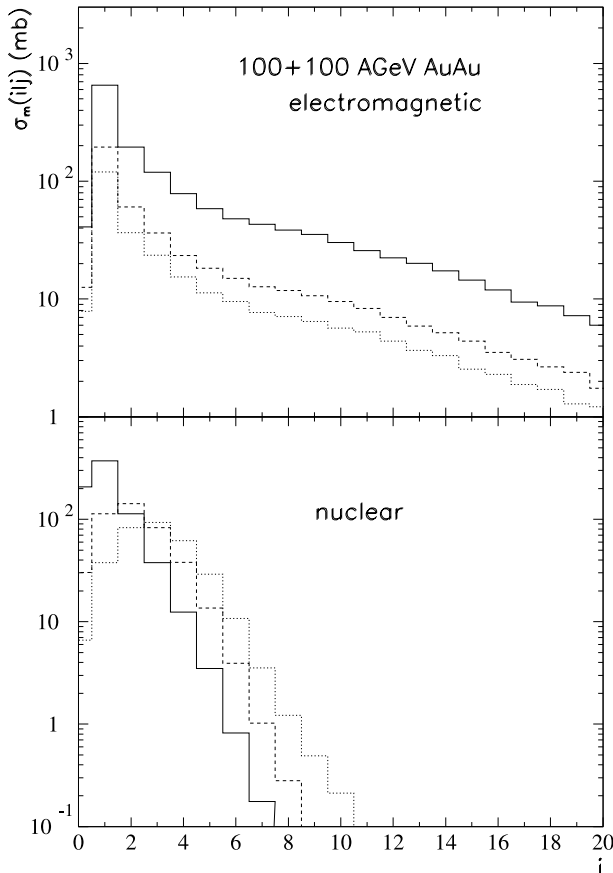
FIG. 10. Mutual electromagnetic $\sigma_m^{ED}(i|j)$ (top) and nuclear $\sigma_m^{nuc}(i|j)$ (bottom) dissociation cross sections for neutron emission in $100+100\,A$ GeV AuAu collisions at the RHIC. The cross section values for $j=1nX$, $2nX$, and $3nX$ are given by the solid, dashed, and dotted histograms, respectively.

FIG. 11. The same as in Fig. 10, but for $2.75+2.75\,A$ TeV PbPb collisions at the LHC.

nent in the plots. Simultaneous GDR excitation in both of the nuclei is a dominant process leading to the mutual dissociation, but it is responsible only for a part of the total mutual dissociation cross section, $\sim 18\%$ at the RHIC, for example. The rest is provided mainly by asymmetric processes, when one of the nuclei is excited in a GDR state, while another nucleus absorbs a photon with the energy above the GDR region, which leads to emission of many neutrons. As seen in Figs. 12 and 13, the probabilities of the simultaneous emission of three and more neutrons are small and such processes with participation of high-energy photons are distributed over the large area in the plots.

For the sake of completeness the cross sections of the mutual dissociation without neutrons emitted from one or both of the collision partners are also included. The rates of such processes, when mainly the proton emission takes place, are small. This is another difference between the electromagnetic and nuclear dissociations. The nuclear interaction events, when only a proton is removed from one or both of the nuclei, are very probable, see Figs. 12 and 13.

VII. CONCLUSIONS

Since its experimental discovery, the process of electromagnetic dissociation of heavy ions has been studied only in
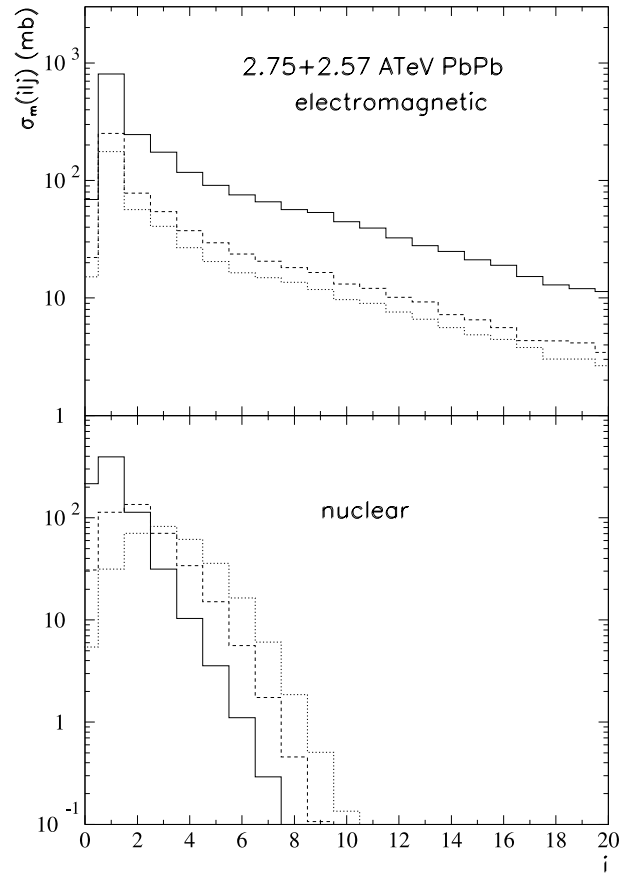
fixed target experiments. In the year 2000 the Relativistic Heavy Ion Collider (RHIC) became operational at BNL and among other experiments the electromagnetic dissociation of ultrarelativistic heavy ions can now be investigated in collider kinematics by means of the zero degree calorimeters (ZDC) [56]. This makes possible the study the mutual heavy-ion dissociation process.

In the present paper the equivalent photon method and the abrasion model for grazing nuclear collisions were extended to the case of mutual dissociation of collision partners. Our numerical results for the total heavy-ion dissociation cross sections are very close to the results of related studies, see Refs. [3,7,11]. Restricting ourselves to the domain of equivalent photon energies below 24 MeV, where only the giant resonance excitations are possible in electromagnetic dissociation, we obtained the cross section of correlated $1n$-$1n$ emission close to that of Ref. [11]. However, as we have found, at collider energies the neutron emission process in mutual electromagnetic dissociation is not entirely exhausted by the simultaneous excitation and decay of the giant resonances in both of the colliding nuclei. Apart from the mutual GDR excitation, asymmetric processes with the GDR excitation in one of the nuclei accompanied by a photonuclear reaction in the other nucleus are very probable. A wide set of photonuclear reactions should be taken into account to obtain a realistic estimation of the mutual dissociation rate.

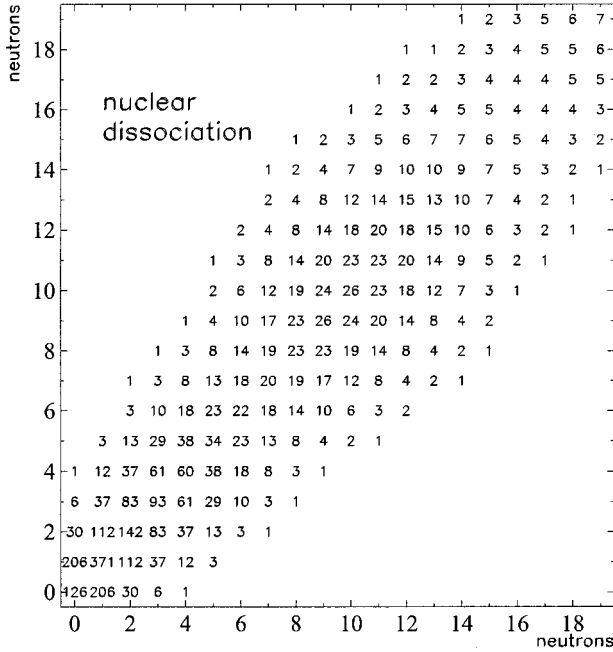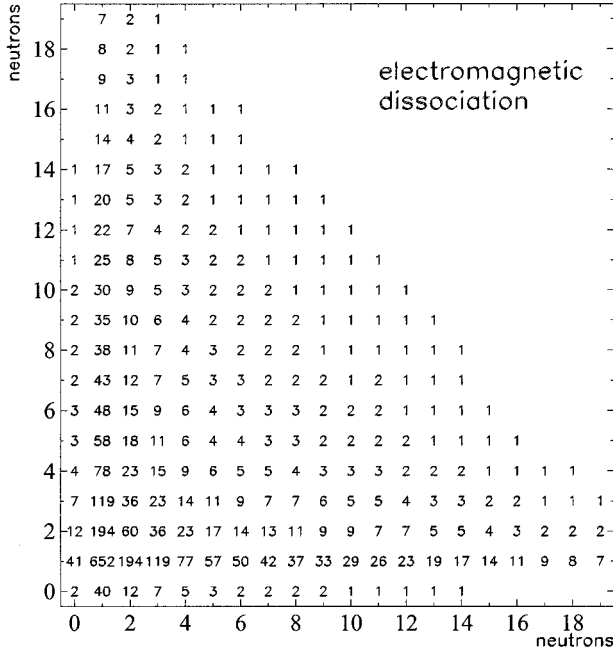As we found, the cross sections of emission of two and

FIG. 12. Mutual dissociation cross sections (mb) for neutron emission $(i,j = 0nX, 1nX, \ldots, 19nX)$ due to electromagnetic $\sigma_m^{ED}(i|j)$ (top panel) and nuclear $\sigma_m^{nuc}(i|j)$ (bottom panel) dissociation in $100 + 100\ A$ GeV AuAu collisions at the RHIC.

FIG. 13. Same as in Fig. 12, but for $2.75 + 2.75\ A$ TeV PbPb collisions at LHC.

especially three neutrons in mutual dissociation are very sensitive to the presence of the next-to-leading-order processes where a collision partner (or even both of the nuclei) absorbs a pair of photons in a collision event. The contribution of multiple photon absorption processes to the total *single* electromagnetic dissociation cross section at ultrarelativistic energies is 1–2 % only. This is very different from the case of *mutual* electromagnetic dissociation where 30–40 % of events are due to multiple photon absorption. Indeed, the main part of mutual dissociation events takes place in close collisions with small $b \gtrsim b_c$, where the probability to absorb
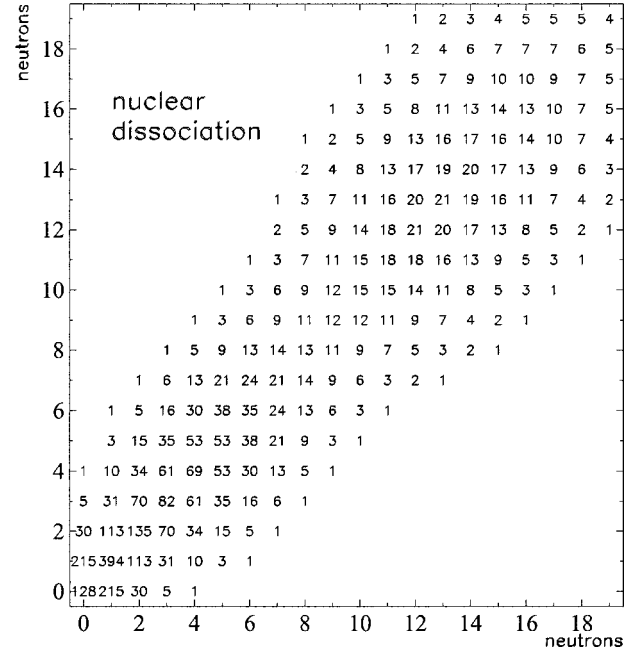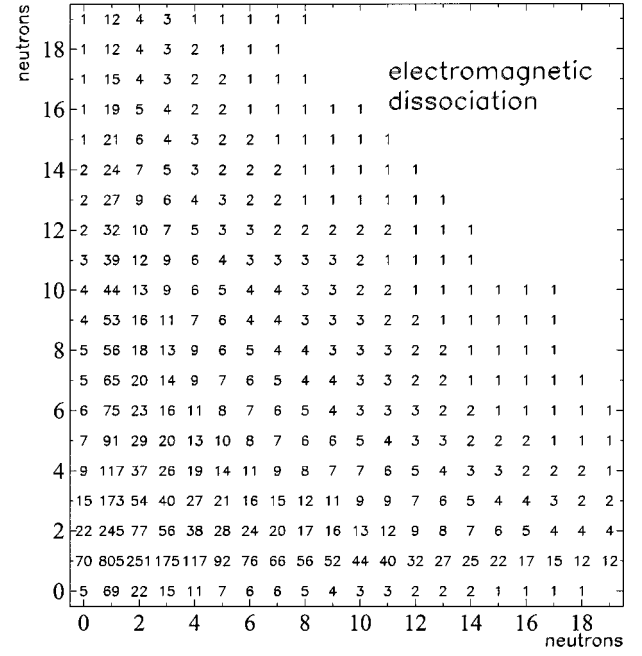
a virtual photon is large, and hence, two or more photons can be absorbed by each of the collision partners.

We have examined the reliability of our results by studying their sensitivity to the variation of input data and parameters. Trying to answer a key question of whether the mutual dissociation cross section can be calculated with high accuracy, we have critically reviewed our model assumptions and the results of previous theoretical and experimental studies of photonuclear reactions and heavy-ion dissociation processes.

The ambiguity in the calculations of the $1n$-$1n$ correlated emission cross section alone, $\sigma(1nX|1nY)$, is found to be up to 15%. This is mainly due to the difference in the values of

the photoneutron cross sections measured in different experiments. However, the ambiguity is lower, $\sim 5-7$ %, if the sum of one and two neutron emission channels $\sigma(1nX|1nY) + 2\sigma(1nX|2nY) + \sigma(2nX|2nY)$ is considered. Therefore, it is a kind of cumulative neutron emission rate that should be used as the luminosity measure at colliders.

We have found several distinctive features of the mutual electromagnetic dissociation process, which are helpful for its experimental identification. Beside the enhancement of $1n$ and $2n$ emission channels, the electromagnetic interaction leads to very asymmetric mutual dissociation channels where only one neutron is lost by one collision partner while many neutrons are lost by another partner. Such a dissociation pattern is very unlikely in grazing nuclear collisions with participation of the strong nuclear forces.

The correlated emission of one or two neutrons in both the forward and backward directions without any additional particles in the midrapidity region can be used as a clear sign of the electromagnetic dissociation of ultrarelativistic heavy ions. The identification of such mutual dissociation events and counting their rates in both arms of ZDC along with the calculation results of the present paper can provide a basis for an absolute luminosity calibration at the RHIC. Similar methods can be used for the ALICE heavy ion experiment [57] planned at the future Large Hadron Collider (LHC) to be built at CERN.

[1] Conceptual design of the Relativistic Heavy Ion Collider (RHIC), BNL-52195 UC-414, 1989.

[2] ALICE, Technical Proposal for A Large Ion Collider Experiment at the CERN LHC, CERN/LHCC/95-71, 1995.

[3] F. Krauss, M. Greiner, and G. Soff, Prog. Part. Nucl. Phys. **39**, 503 (1997).

[4] G. Baur, K. Hencken, and D. Trautmann, J. Phys. G **24**, 1657 (1998).

[5] I. A. Pshenichnov, I. N. Mishustin, J. P. Bondorf, A. S. Botvina, and A. S. Iljinov, Phys. Rev. C **60**, 044901 (1999).

[6] I. A. Pshenichnov, I. N. Mishustin, J. P. Bondorf, A. S. Botvina, and A. S. Iljinov, Phys. Rev. C **57**, 1920 (1998).

[7] A. J. Baltz, M. J. Rhoades-Brown, and J. Weneser, Phys. Rev. E **54**, 4233 (1996).

[8] J. P. Bondorf, A. S. Botvina, A. S. Iljinov, I. N. Mishustin, and K. Sneppen, Phys. Rep. **257**, 133 (1995).

[9] A. J. Baltz and S. N. White, RHIC/DET-20, preprint BNL-63127 (unpublished).

[10] S. N. White, Nucl. Instrum. Methods Phys. Res. A **409**, 618 (1998).

[11] A. J. Baltz, C. Chasman, and S. N. White, Nucl. Instrum. Methods Phys. Res. A **417**, 1 (1998).

[12] C. J. Benesh and J. L. Friar, Phys. Rev. C **50**, 3167 (1994).

[13] K. Hencken, D. Trautmann, and G. Baur, Phys. Rev. C **53**, 2532 (1996).

[14] K. Hencken, D. Trautmann, and G. Baur, Z. Phys. C **68**, 473 (1995).

[15] J. D. Jackson, *Classical Electrodynamics*, 2nd ed. (Wiley, New York, 1975).

[16] W. J. Llope and P. Braun-Munzinger, Phys. Rev. C **41**, 2644 (1990).

[17] C. A. Bertulani and G. Baur, Phys. Rep. **163**, 299 (1988).

[18] J. Hüfner, K. Schäfer, and B. Schürmann, Phys. Rev. C **12**, 1888 (1975).

[19] L. F. Oliveira, R. Donangelo, and J. O. Rasmussen, Phys. Rev. C **19**, 826 (1979).

[20] J.-J. Gaimard and K. H. Schmidt, Nucl. Phys. **A531**, 709 (1991).

[21] M. Gazdzicki and O. Hansen, Nucl. Phys. **A528**, 754 (1991).

[22] C. J. Benesh, B. C. Cook, and J. P. Vary, Phys. Rev. C **40**, 1198 (1989).

[23] A. Veyssière, H. Beil, R. Bergère, P. Carlos, and A. Leprêtre, Nucl. Phys. **A159**, 561 (1970).

[24] A. Leprêtre, H. Beil, R. Bergère, P. Carlos, J. Fagot, A. De Miniac, and A. Veyssière, Nucl. Phys. **A367**, 237 (1981).

[25] A. Leprêtre, H. Beil, R. Bergère, P. Carlos, J. Fagot, A. De Miniac, and A. Veyssière, Nucl. Phys. **A390**, 221 (1982).

[26] R. R. Harvey, J. T. Caldwell, R. L. Bramblett, and S. C. Fultz, Phys. Rev. **136**, 126 (1964).

[27] B. L. Berman and S. C. Fultz, Rev. Mod. Phys. **47**, 713 (1975).

[28] S. S. Dietrich and B. L. Berman, At. Data Nucl. Data Tables **38**, 199 (1988).

[29] J. D. T. Arruda-Neto, S. Simionatto, V. P. Likhachev, F. Garcia, J. Mesa, A. Deppman, O. Rodriguez, and E. Guzmàn, Nucl. Phys. **A638**, 701 (1998).

[30] E. Wolynec, A. R. V. Martinez, P. Gouffon, Y. Miyao, V. A. Serrao, and M. N. Martins, Phys. Rev. C **29**, 1137 (1984).

[31] B. L. Berman, R. E. Pywell, S. S. Dietrich, M. N. Thompson, K. G. McNeill, and J. W. Jury, Phys. Rev. C **36**, 1286 (1987).

[32] S. N. Beljaev and V. A. Semenov, Izv. Ross. Akad. Nauk, SSSR, Ser. Fiz. **55(5)**, 953 (1991).

[33] V. V. Varlamov, N. G. Efimkin, B. S. Ishkhanov, and V. V. Sapunenko, Jadernye Konstanty (Nuclear Constants) **1**, 52 (1993) [in Russian].

[34] P. G. Young, E. D. Arthur, and M. B. Chadwick, in *Nuclear Reaction Data and Nuclear Reactors*, edited by A. Gandini and G. Reffo (World Scientific, Singapore, 1998), Vol. I, p. 227.

[35] M. B. Chadwick and P. G. Young, Acta Phys. Slov. **45**, 633 (1995).

[36] M. B. Chadwick, P. Obložinsky, G. Reffo, and P. E. Hodgson, Phys. Rev. C **44**, 814 (1991).

[37] A. S. Iljinov, I. A. Pshenichnov, N. Bianchi, E. De Sanctis, V. Muccifora, M. Mirazita, and P. Rossi, Nucl. Phys. **A616**, 575 (1997).

[38] V. Muccifora, N. Bianchi, A. Deppman, E. De Sanctis, M. Mirazita, E. Polli, P. Rossi, R. Burgwinkel, J. Hannappel, F. Klein, D. Menze, W. J. Schwille, and F. Wehnes, Phys. Rev. C **60**, 064616 (1999).

[39] R. Engel, J. Ranft, and S. Roesler, Phys. Rev. D **55**, 6957 (1997).

[40] N. Bianchi, E. De Sanctis, M. Mirazita, and V. Muccifora, Phys. Rev. C **60**, 064617 (1999).

[41] A. V. Ignatyuk, G. N. Smirenkin, and A. S. Tishin, Yad. Fiz. **21**, 485 (1975).

[42] A. V. Ignatyuk, K. K. Istekov, and G. N. Smirenkin, Yad. Fiz. **29**, 875 (1979).

[43] A. S. Iljinov, M. V. Mebel, N. Bianchi, E. De Sanctis, C. Guaraldo, V. Lucherini, V. Muccifora, E. Polli, A. R. Reolon, and P. Rossi, Nucl. Phys. **A543**, 517 (1992).

[44] A. M. van den Berg, D. Chmielewska, J. A. Bordewijk, S. Brandenburg, A. van der Woude, Y. Blumenfeld, N. Frasaria, J. C. Roynette, J. A. Scarpaci, T. Suomijärvi, N. Alamanos, F. Auger, A. Gillibert, P. Roussel-Chomaz, J. Blomgren, L. Nilsson, N. Olsson, and R. Turcotte, Nucl. Phys. **A578**, 238 (1994).

[45] R. Alarcon, P. L. Cole, D. S. Dale, P. T. Debevec, and L. J. Morford, Phys. Rev. C **43**, R2470 (1991).

[46] R. F. Askew and A. P. Batson, Nucl. Phys. **20**, 408 (1960).

[47] F. Tagliabue and J. Goldemberg, Nucl. Phys. **23**, 144 (1961).

[48] G. A. Chekomazov and M. H. Urin, Phys. Lett. B **354**, 7 (1995).

[49] T. Aumann, C. A. Bertulani, and K. Sümmerer, Phys. Rev. C **51**, 416 (1995).

[50] J. W. Norbury and L. W. Townsend, Phys. Rev. C **42**, 1775 (1990).

[51] A. Grünschloss, K. Boretzky, T. Aumann, C. A. Bertulani, J. Cub, W. Dostal, B. Eberlein, Th. W. Elze, H. Emling, J. Holeczerk, R. Holzmann, M. Kaspar, J. V. Kratz, R. Kulessa, Y. Leifels, A. Leistenschneider, E. Lubkiewicz, S. Mordechai, I. Peter, P. Reiter, M. Rejmund, H. Simon, K. Stelzer, A. Surowiec, K. Sümmerer, J. Stroth, E. Wajda, W. Walus, S. Wan, and H. J. Wollersheim, Phys. Rev. C **60**, 051601(R) (1999).

[52] Particle Data Group, C. Caso *et al.*, Eur. Phys. J. C **3**, 1 (1998).

[53] H. Dekhissi, G. Giacomelli, M. Giorgini, G. Mandrioli, S. Manzoor, L. Patrizii, V. Popa, P. Serra, and V. Togo, Nucl. Phys. **A662**, 207 (2000).

[54] J. C. Hill, A. Petridis, B. Fadem, and F. K. Wohn, Nucl. Phys. **A661**, 313 (1999).

[55] C. A. Bertulani and V. Yu. Ponomarev, Phys. Rep. **321**, 139 (1999).

[56] C. Adler, A. Denisov, E. Garcia, M. Murray, H. Stroebele, and S. White, nucl-ex/0008005 (to be published).

[57] ALICE Collaboration, J. Schukraft *et al.*, Technical Design Report of the Zero Degree Calorimeter (ZDC), CERN/LHCC 99-5, ALICE TDR 3, 1999.